4. S. Patankar and D. Spaulding, Thermo- and Mass-Exchange in Boundary Layers [Russian translation], Énergiya, Moscow (1971).
5. R. W. MacCormack, The Effect of Viscosity in Hypervelocity Impact Cratering, Paper No. 69, AIAA, New York (1969).
6. L. V. Gorish and G. Yu. Stepanov, Separated and Cavitating Flows: Basic Properties and Computational Models [in Russian], Nauka, Moscow (1990).
7. G. N. Abramovich (ed.), Theory of Turbulent Jets, 2nd edn., revised and corrected [in Russian], Nauka, Moscow (1984).

NUMERICAL MODELING OF MACH REFLECTION FOR SOLITARY WAVES

O. A. Serebrennikova and A. M. Frank

UDC 532.59

It is well known that when a surface solitary wave is incident on a vertical wall, located under an angle to the wave front, one can have either regular reflection, when only two waves are observed — the incident and the reflected, with their angles and amplitudes coinciding, or Mach reflection, when a ternary nonsymmetric configuration is generated. The studies [1-5] are devoted to investigating this phenomenon.

Perroud (see [3, 6]) has conducted experiments on wave reflection of dimensionless amplitude a = 0.08-0.38 in a wide range of incidence angles. Perroud observed that regular reflection is always realized for incidence angles $\psi_i \geqslant 45^\circ$, while Mach reflection occurs for $\psi_i \leqslant 45^\circ$. Quantitative characteristics of amplitudes and phases were also determined for wave reflection and Mach steps. According to Perroud's data, these parameters depend on the wave angle of incidence on the wall and are practically independent of its amplitude.

For low amplitude waves there exist theoretical results [2] on the resonance interaction of three solitary waves, providing, in particular, for $t \to \infty$ the asymptotic solution for Mach reflection problems. In that study it was obtained that the critical incidence angle ψ_i^*, distinguishing the two types of reflection, depends on the wave amplitude and equals $\sqrt{3a}$. The parameters of the ternary configuration also depend not only on the wave angle of incidence, but also on is amplitude. The predicted wave amplitude at the wall also differs substantially from experiment, reaching 4a in the Miles solution at the critical angle of incidence $\psi_i = \sqrt{3a}$.

In [4] this effect is modeled numerically with the use of approximate long-wave equations of low amplitude. The calculations were carried out for a = 0.05 and, on the whole, are in fair agreement with the Miles theory.

Specific experiments were carried out [3] so as to verify the theoretical model [2]. The reflection was treated of waves of amplitudes a = 0.1-0.15 for different angles. As a result of handling measurement data the author has expressed doubts concerning the validity of applying the Miles method to this problem. Thus, it must be recognized that a number of problems still remain open in this case.

In the present study we present results of a numerical investigation of a solitary wave reflection from a vertical wall for different amplitudes and angles of incidence. As mathematical models we use two discrete models of an incompressible fluid. The study substantially augments and refines the preliminary results, published in [7], of calculations for this problem, where a cruder grid was used and a solution was obtained for relatively small values of physical time.

1. Three-Dimensional Discrete Model. The given model is a generalization of the discrete model [8] to the three-dimensional case. The three-dimensional problem is considered of the interaction of a solitary wave over an even bottom with a rigid vertical wall, placed at an angle to the front. The z axis is directed upwards, and z = 0 corresponds to a flat unperturbed free surface. In the region Ω occupied by the fluid one introduces the regular grid

$$\Omega_h = \{\mathbf{r}_\alpha = (x_\alpha, y_\alpha, z_\alpha) \mid \alpha = (i, j, k),\ i = 1, ..., M,\ j = 1, ..., N,\ k = 1, ..., L\},$$

Krasnoyarsk. Translated from Prikladnaya Mekhanika i Tekhnicheskaya Fizika, No. 5, pp. 15-24, September-October, 1993. Original article submitted August 24, 1992.

 0021-8944/93/3405-0610$12.50

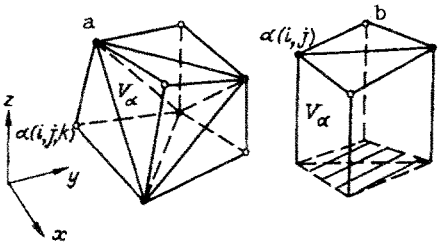

Fig. 1

In this case k = 1 and k = L correspond, respectively, to nodes located on the bottom and on the free surface, and j = 1 corresponds to nodes on the vertical wall. The unit cell is an irregular dodecahedron with vertices at grid nodes, whose boundaries form triangles (Fig. 1a). It is easily seen that the unit cells of the grid divide the whole region Ω into elementary volumes without cavities and intersections. In this case the free boundary is a piecewise-linear surface of triangular elements.

We assume that on the grid nodes are located material particles, in which is concentrated the whole mass of the medium, while the particle mass with subscript $\alpha = (i, j, k)$ is determined in the form

$$m_\alpha = \frac{\rho}{8} \sum_{\beta \in N_\alpha} V_\beta,$$

where V_α is the volume of the unit cell with subscript α; $N_\alpha = \{(i - \gamma_1, j - \gamma_2, k - \gamma_3) | \gamma_s = 0, 1\}$ is the set of subscripts of cells adjacent to it, and ρ is the fluid density.

The next step is the formulation of the kinematic restriction on possible particle motions, which for a fluid is the incompressibility condition. In the given discretization the natural incompressibility condition is the constancy condition of the volumes of all unit cells of the grid during the process of particle motions:

$$V_\alpha = V_\alpha^0 = \text{const}. \tag{1.1}$$

The unit cell volume V_α is expressed in terms of the vertex coordinates, therefore conditions (1.1) are the usual holonomic relations.

Furthermore, since the gravitational wave problem is being investigated it is necessary to somehow introduce the gravity force into the treatment. The simplest method, usually employed in Lagrange methods, consists of the gravity force F_α, acting on each particle, having the form

$$F_\alpha = m_\alpha \mathbf{g}. \tag{1.2}$$

However, this gravity force, unlike the continuous case, is, generally speaking, in disagreement with the incompressibility condition (1.1) in the sense that, for example, a "fluid" layer of constant depth is found in equilibrium only in the case of a rectangular grid Ω_h. For an arbitrary grid equilibrium breaks down, i.e., the reactive forces (1.1) are incapable of compensating the gravity force (1.2) for all particles simultaneously. As applied to the equations of hydrodynamics, this situation implies an inconsistency between the pressure gradient approximation and the gravitational potential gradient. Therefore, similarly to the two-dimensional case [8], in the present study the gravity force is introduced as follows. The potential energy of the system of particles is assumed equal to the potential energy of a fluid layer with a free boundary:

$$\Pi = \frac{\rho g}{2} \iint \eta^2 dx dy. \tag{1.3}$$

Here η is the elevation from the resting level of the piecewise-linear free surface of the discrete medium. Clearly, by this definition the potential energy depends only on the coordinates of the surface particles (the shape of this function is copied explicitly) and the potential energy minimum, i.e., stable equilibrium of the layer, is reached at $\eta = 0$ for any grid.

Thus, as a model of the original problem one obtains a finite system of material particles with kinetic energy

$$T = \frac{1}{2} \sum_\alpha m_\alpha (u_\alpha^2 + v_\alpha^2 + w_\alpha^2),$$

potential energy (1.3), and holonomous relations (1.1), whose motion is described by the classical Lagrange equations. Due to the nonflow condition of particles located at the bottom and on the wall, unlike particles in the interior they have only two degrees of freedom at the bottom and wall planes, respectively.

Introducing for all particles generalized coordinates q_n, coinciding for interior particles with Cartesian coordinates, the system Lagrangian can be written in the form

$$L = \frac{1}{2}\sum_n m_n \dot{q}_n^2 - \Pi + \sum_\alpha \lambda_\alpha (V_\alpha - V_\alpha^0),$$

where λ_α is a Lagrange multiplier. The Lagrange equations are

$$m_n \dot{v}_n = \sum_\alpha \lambda_\alpha \frac{\partial V_\alpha}{\partial q_n} - \frac{\partial \Pi}{\partial q_n}, \quad \dot{q}_n = v_n, \quad V_\alpha = V_\alpha^0. \tag{1.4}$$

We note that by the corresponding theorems of classical mechanics the system (1.4) conserves the total energy H = T + Π = const for any number of degrees of freedom. Moreover, in the absence of rigid walls and for g = 0 the system is also subject to conservation laws of momentum and angular momentum due to the invariance of relations (1.1) with respect to translational shift and rotation. Conservation of the total fluid volume is guaranteed by conditions (1.1).

By the method of introducing unit cells, as described above, it is seen that the grid nodes are nonuniform. Thus, the bright nodes (Fig. 1a) change the volume of a single tetrahedron in each unit cell, while the dark ones correspond to four. Therefore, the symmetrization condition of incompressibility was used in the calculations – the dark and bright nodes change roles at each step in time.

2. Discrete Model of Shallow Water. This model is a generalization of the one-dimensional nonlinear-dispersion model of shallow water [9] to the spatial case. Unlike Sec. 1, here the grid consists of a single layer of unit cells in depth. Each unit cell V_α, $\alpha = (i, j)$ is a combination of two triangular prisms with lateral boundaries perpendicular to the bottom (Fig. 1b). The Lagrangian particles, serving simultaneously as unit cell vertices, are located only on the free surface. The basic assumption is that the horizontal components of the fluid velocity are independent of depth, while due to the continuity equation the vertical velocity varies linearly from zero at the bottom to some finite value at the free surface. In this case the kinetic energy of the discrete system can be written in the form

$$T = \frac{1}{2}\sum_\alpha m_\alpha (u_\alpha^2 + v_\alpha^2 + \frac{1}{3} w_\alpha^2),$$

where $m_\alpha = \frac{\rho}{4}\sum_{\beta \in N_\alpha} V_\beta$, and the factor 1/3 appears due to the integration of the linear term over z. The incompressibility condition has the same shape (1.1), though the dependence of V_α on the particle coordinates is, naturally, different. The introduction of a potential energy, the statement of boundary conditions at the rigid walls, and the symmetrization scheme are carried out here in exactly the same way as in Sec. 1. The Lagrange equations differ from (1.4) only by the presence of the factor 1/3 in $\dot{w}_\alpha$. For the one-dimensional discrete model of shallow water [9] it has been shown that in the case of an even bottom it is a complete conservative approximation of the Green–Naghdi equations [10] in Lagrange coordinates. For the two-dimensional model provided here it can be shown that for an even bottom it is a complete conservative decoupling scheme of the same equations, while the conservation laws are satisfied at each half-step. In the following the discrete models of Secs. 1, 2 are denoted as models 1 and 2. The algorithm of [11] was used for numerical implementation of these models.

3. Calculation Results. All calculations described below were performed for the following values of depth H = 1, density ρ = 1, and acceleration g = 1, which is equivalent to the introduction of dimensionless variables by means of the scales H, $\sqrt{gH}$, ρ, in which case the Froude number is Fr = 1. Both models were first tried on the problem of a soliton traveling over an even bottom. The calculations have shown that here, as in the first case of discrete models of lesser dimensionality, solitary waves are realized even on a quite crude grid. Due to the conservation properties of the discrete model and of the numerical algorithm these waves propagate with constant mean amplitude, energy, and phase velocity. The wave amplitude was determined by means of quadratic interpolation along three adjacent particles, and the mean phase velocity – by the distance traversed by the wave during Δt = 20. For a soliton

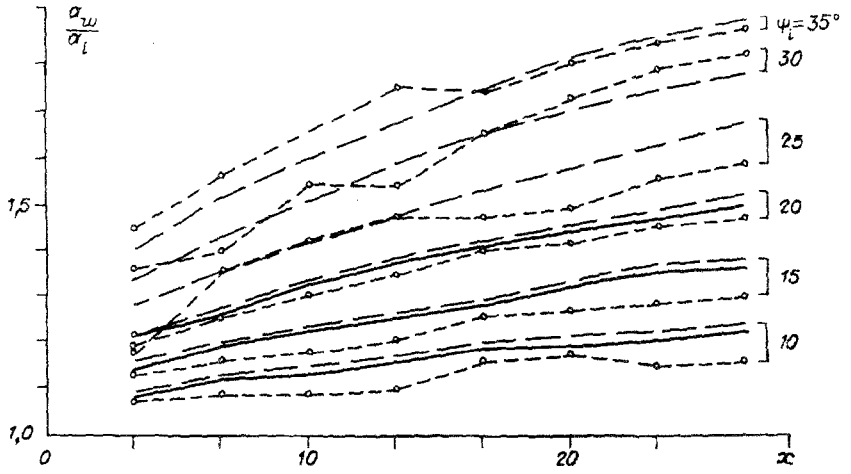

Fig. 2

of amplitude a = 0.2 on a grid with unit cell sizes $h_1 = h_2 = 1$, $h_3 = 0.5$ (for model 1) and for a time step $\tau = 0.5$ the shape of the steady-state soliton and its mean phase velocity differ from the corresponding quantities for a classical Rayleigh soliton by no more than 3 and 0.1% (for model 1), 0.5 and 0.03% (for model 2). The small oscillations in instantaneous amplitude and phase velocity values, related to the discrete representation of the wave, do not exceed 1% and do not have a tendency to increase. In the following calculations the spatial and temporal step values were selected close to those given above.

Next we modeled the experiment [3], in which was investigated the initial stage of solitary wave reflection from an oblique wall. In the experiment this wall was placed at a varying angle to the lateral basin wall at some distance from the wave generator. The x axis is directed along the oblique wall, and x = 0 corresponds to the break point. In the numerical calculations the experimental scheme was repeated in the parts concerning the basin geometry (besides the initial portion with the wave generator), the arrangement of detectors of the even fluid, and the data analysis. The difference consisted only of the initial wave generation, which was here simply assigned at the input portion as initial values from an approximate solution [12]. The comparison results between the calculated and experimental data are given below.

In Fig. 2 is shown the x-dependence of the wave amplitude at the wall a_w, relative to the incident wave amplitude a_i, for $a_i = 0.1$ and various incidence angle of the wave ψ_i. In Figs. 2-4 the points connected by short dashes are experiment, and the solid and dashed lines are models 1 and 2. Here and later the incidence angle ψ_i and the reflection angle ψ_r are understood to be the angles between the wave vector of the corresponding wave and the normal to the wall. It is seen that the quantitative difference is no more than 7%, though for small angles the calculated amplitude values are systematically larger than the experimental values. With the purpose of further verification of the calculation accuracy, calculations were performed by model 2 for ψ_i = 10 and 35° on twice as small a grid (153 × 53 instead of 77 × 27 nodes) and twice as small a step in time ($\tau = 0.25$). The dependencies obtained in this case differed from the calculations given by less than 1%. Figure 3 shows for $a_i = 0.15$ the y-dependence of the maximum elevation of the free surface relative to a_i, constructed from the fixed detectors shown, located on a straight line perpendicular to the wall at x = 16.7. It is seen that for ψ_i = 30 and 35° the agreement between calculation and experiment is very good, while for small angles the difference reaches 10%. We note that for small angles the experimental profiles have, for some reason, a nonsmooth shape. This was not commented upon in [3], though the resolution of detectors exceeded by one order the scale of fluctuation data. In Fig. 4 we show characteristic dependencies of the shape generated during reflection of the wave configuration. In the calculation, as well as in the experiment, the level detector garlands were located on a straight line perpendicular to the wall at x = 23.3. By τ_* we denote the time difference between the passage of the wave crest through a detector with coordinate y_i and a detector at the wall at $y_0 = 0$. Here, following [3], τ_* was determined by means of the correlation function

$$R_i(\tau) = \sum_{t_0-T/2}^{t_0+T/2} \eta_0(t)\,\eta_i(t+\tau), \quad R_i(\tau_*) = \max_{\tau} R_i(\tau),$$

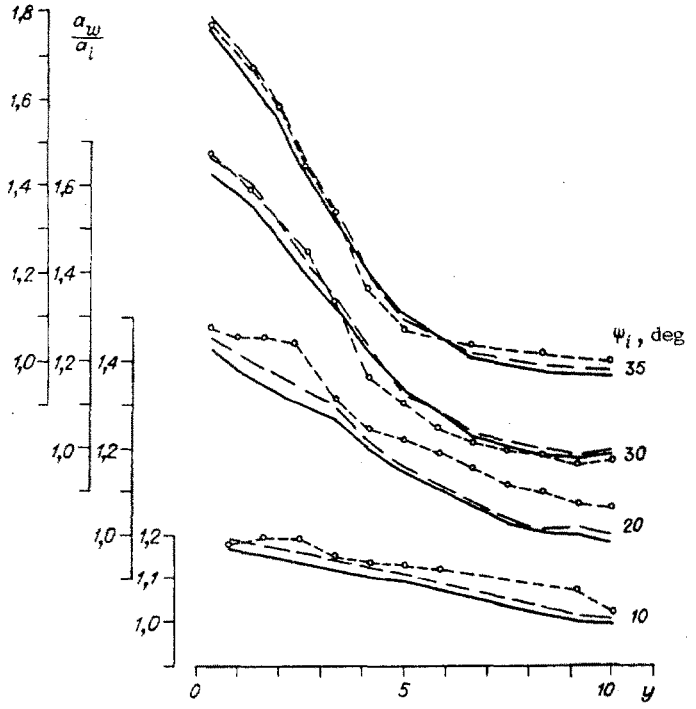

Fig. 3

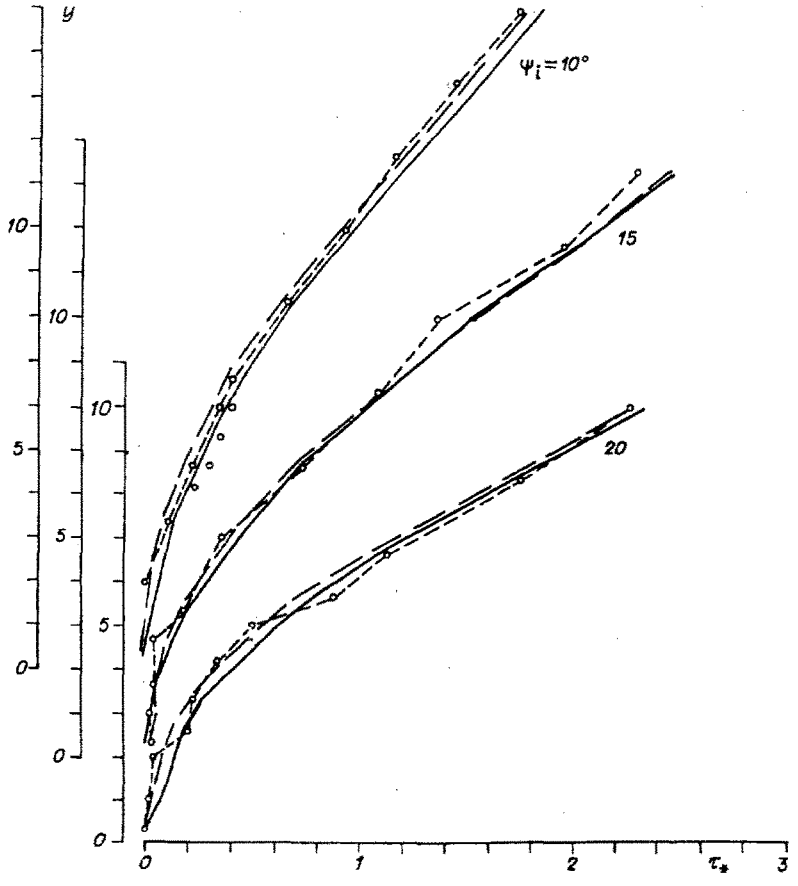

Fig. 4

where $\eta_0(t)$, $\eta_i(t)$ are the recorded levels at the corresponding detectors, $t_0 = \arg\max_t \eta_0(t)$, and the window size is T = 3.65. The experimental points are given for $a_i = 0.15$ for three ψ_i values. On the whole it can be stated that the calculation results in both models are in satisfactory agreement between them and with the experimental results.

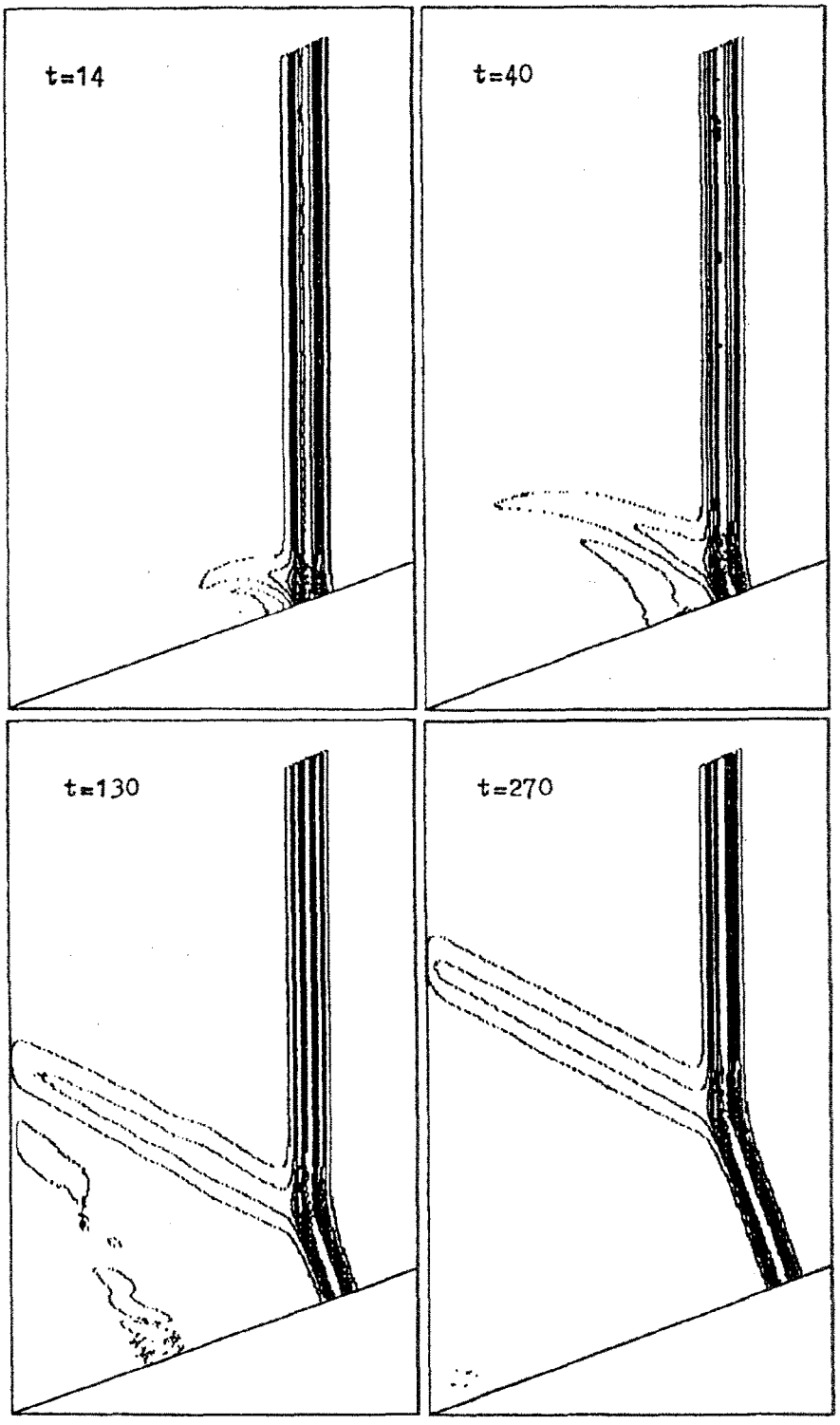

Fig. 5

The next substantial series of calculations is devoted to studying the time evolution of the wave configuration up to the steady state. In this case, as follows from theory [2] and from numerical calculations, for regular reflection there exists a truly stationary V-shaped configuration, moving along the wall with a constant velocity. For a ternary Mach configuration an exception to stationarity occurs only for a reflection angle ψ_r and wave amplitudes, and a Mach portion length continuing to increase with time. The detection time varies from several dozen dimensionless units for regular reflection to thousands and more for a ternary configuration. Therefore, we used in the calculation a moving computational region in the form of a parallelogram, which was displaced along the wall immediately behind the wave, while the initial data appeared in the form of a solitary wave, incident on the

oblique wall. In Fig. 5 we provide an example of the time evolution of a ternary configuration for a wave with amplitude $a_i = 0.3$ for $\psi_i = 20°$. Here the nonflow condition was imposed at the wall, on part of the upper boundary was assigned a traveling solitary wave from the parallel solution of the problem of one lesser dimensionality, while no further conditions were imposed on the remaining boundaries, so that from the point of view of the equations of hydrodynamics the boundary corresponds to the given hydrostatic pressure.

The calculations were carried out on nonuniform grids from 50 × 41 × 3 (model 1) to 131 × 131 (model 2) nodes. Depending on the type of model and on the problem parameters, the sizes of the computational region were selected from 48 × 104 to 197 × 220 units. The computation time of a single version up to the steady state was from 2 to 20 h on a PC/AT 386/33. The incident wave amplitude varied from 0.1 to 0.3. To compare with the results of [4] we also performed two calculations for $a_i = 0.05$. Large amplitudes were not considered, since even for $a_i = 0.3$ the amplitude of the Mach portion exceeds substantially the critical height for a solitary wave 0.83 for some incidence angles, which must in reality lead to its collapse. An accurate calculation of waves with an amplitude less than 0.05 requires a too large computational region, also increasing the time of reaching the steady state, so that the total computational time increases to impractical values.

The basic problem in this series is clarifying the dependencies of the wave amplitude at the wall a_w, the reflected wave amplitude a_r, and the reflection angle ψ_r on the incident wave amplitude a_i and on the angle of incidence ψ_i. Figure 6 shows the calculated dependence of ψ_r on ψ_i. For model 1 $a_i = 0.097$, 0.186 (points 1, 2), and for model 2 $a_i = 0.05$, 0.097, 0.186, 0.3 (points 3-6). The points 7 provide the calculation results of [4] for $a_i = 0.05$. The dashed lines for each of the a_i values considered illustrate the theoretical Miles dependence [2]:

$$\psi_r = \begin{cases} \sqrt{3a_i} & \text{for} \quad \psi_i < \sqrt{3a_i}, \\ \psi_i & \text{for} \quad \psi_i \geq \sqrt{3a_i}. \end{cases}$$

It is seen that for $a_i = 0.05$ the two calculations by model 2, representing both types of reflection, are in good agreement with the results of [4] and in fair agreement with the Miles theory. At large amplitudes the theory provides an enhanced value of the reflection angle, though even for $a_i = 0.097$ the theoretical estimate of the reflection angle is still quite valid. A stronger nonlinearity also leads to a characteristic nonmonotonic dependence of the reflection angle on the angle of incidence. In this case the curve minima correspond to a ternary configuration with a maximum amplitude of the Mach portion (Fig. 7).

Figure 7 shows the calculated value of the reflected wave amplitude a_r and the Mach portion at the wall a_w, relative to a_i, as a function of the variable $\psi_i/\sqrt{3a_i}$. Also given are the results of [4] for $a_i = 0.05$ and the theoretical results [2], providing universal dependencies in these variables (dashed lines). The notations are the same as in Fig. 6. It is seen from Fig. 7 that an increase in nonlinearity leads to a substantial quantitative deviation from the universal Mach dependencies, but the qualitative character still holds. Most interesting is here the effect of resonance amplification of wave amplitude at the wall, reaching the value of $3.5a_i$ in the calculations. It must be noted that, since the peaks are very sharp, it cannot be excluded that not very large values are obtained in the calculations for low amplitudes. Nevertheless, the value of $3.5a_i$ substantially exceeds the maximum splash value of the wave during ordinary rolling onto the vertical roll at a right angle, which, as well known, practically coincides with the result of the linear theory $2a_i$. In the Perroud experiments (see [3, 6]) for ternary configurations the ratio a_w/a_i did not exceed 2. It was noted in [3] that capillary effects, as well as wave collapse, are explicitly present in these experiments. Another reason for absence of observations of this effect is, most probably, the fact that, judging from the present calculations, a ternary configuration with a maximum amplitude of the Mach portion is established further away than for all the remaining ones, and, depending on the amplitude, this time consists of 500 and more dimensionless units. Following this time the incident wave traverses more than 500 depths, which is hardly possible to implement under laboratory conditions. Moreover, in the given calculations the minimum time of reaching the ternary configuration parameters was about 200 for $a_i = 0.3$, $\psi_i = 20°$ (see Fig. 5), so that obtaining a complete steady-state ternary configuration in a laboratory experiment is, obviously, quite problematic. On the other hand, this relation between scales is quite realistic under natural conditions, so that the effect of resonance amplification predicted in [2] during wave rolling onto a shore at an angle can even be of practical interest, such as in, say, tsunami waves.

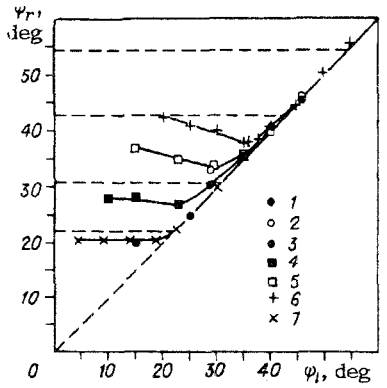

Fig. 6

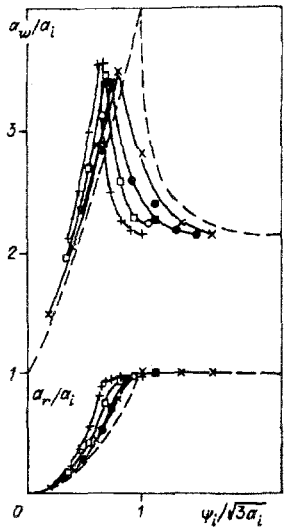

Fig. 7

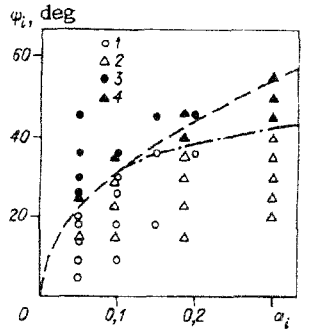

Fig. 8

A qualitative distinction between the results given and the asymptotic theory [2] is that for increasing angle ψ_i and following the curve peak in Fig. 7 the wave configuration may not evolve with time into a ternary configuration, but remains slightly nonsymmetric, and transforms to symmetric only with further increase in ψ_i. As seen from Figs. 6, 7, in these cases the reflection angle ψ_r exceeds ψ_i by (1-2)°, while the reflected wave amplitude is somewhat smaller than a_i.

The dependence of the reflected wave amplitude a_r on the angle of incidence for a ternary configuration is also qualitatively, and for low amplitudes even quantitatively, close to the Miles quadratic dependence $a_r = \psi_i^2/3$, though with some amplitude-dependent coefficient. For $a_i = 0.3$, for example, the calculated points are very well located on the curve $a_r = 0.62\psi_i^2$. A decrease in the amplitude a_r with decreasing ψ_i was also observed in the Perroud experiments.

Finally, Fig. 8 shows a diagram in the parameter plane a_i, ψ_i, taken from [4] and augmented with the present calculations. Here the points 1, 2 correspond to irregular reflection, and 3, 4 to regular reflection (the points 1, 3 – [4], the points 2, 4 – present study). In the present study reflection was assumed to be irregular if the steady-state value of a_r was less than $0.95a_i$. The dashed line is the theoretical curve [2] for the critical angle separating the two types of reflection $\psi_i^* = \sqrt{3a_i}$. Good agreement with theory is observed for amplitudes $a_i < 0.1$. For larger a_i the dash-dot curve corresponds better to the calculation results. This dependence increases substantially more slowly than the quadratic root, and for moderate amplitudes provides a value of the critical angle similar to the experimental data of Chen and Perroud given in [6], where the values 40 and 45°, respectively, were obtained, while the Perroud estimate did not exceed a_i.

The results provided of numerical experiments, along with verifying the existence of ternary configurations in the case of substantially nonlinear equations, as well as the explanation of some quantitative dependencies, are, it seems to us, further arguments concerning the validity of the linear theory [2] in describing Mach reflection of solitary waves at low amplitudes. Doubts concerning this fact were expressed, in particular, in [3]. The main argument is absence in the experiments of resonance amplification of wave amplitudes at the wall. Fair agreement with the experimental results [3] has been obtained in the present study. As seen from Fig. 2, the dependence of a_w on ψ_i for fixed x values in the calculations is also monotonically increasing; however, as follows from the calculations results, this only implies shortness of the times considered. Resonance amplification occurs substantially later, and the size of the experimental basin must be increased by an order of magnitude so as to observe it.

LITERATURE CITED

1. P. H. Perroud, "The solitary wave reflection along a straight vertical wall at oblique incidence," PhD Thesis, UC Berkeley (1957).
2. J. W. Miles, "Resonantly interacting solitary waves," J. Fluid Mech., 79, Part 1 (1977).

3. W. K. Melville, "On the Mach reflexion of a solitary wave," J. Fluid Mech., 98, Part 2 (1980).
4. M. Funakoshi, "Reflexion of obliquely incident solitary waves," J. Phs. Soc. Jpn., 49, No. 6 (1980).
5. G. S. Khakimzyanov, "Numerical simulation of adaptive grids of three-dimensional fluid flows with surface waves," in: Proc. All-Union Conf. Numerical Methods in Problems of Wave Hydrodynamics [in Russian], VTs SO AN SSSR, Krasnoyarsk (1991).
6. R. L. Wiegel, Oceanographical Engineering, Prentice-Hall, Englewood Cliffs, NJ (1964).
7. V. G. Isaev, V. Yu. Karev, L. A. Kompaniets, et al., "Numerical modeling in problems of wave hydrodynamics," Preprint, Krasnoyarsk (1990).
8. A. M. Frank, "Numerical modeling of surface solitary waves within a discrete model of an incompressible fluid," Prikl. Mekh. Tekh. Fiz., No. 3 (1989).
9. A. M. Frank, "Discrete shallow water model," in: Intern. Workshop Laboratory Modeling of Dynamic Processes in Oceans, Vladivostok (1991).
10. A. E. Green and P. M. Naghdi, "A derivation of equations for wave propagation in water of variable depth," J. Fluid Mech., 78, 237-246 (1976).
11. A. M. Frank, "Completely conservative numerical algorithm for discrete models of an incompressible fluid," in: Modeling in Mechanics [in Russian], Vol. 1(18), No. 5, VTs SO AN SSSR, Novosibirsk (1987).
12. L. V. Ovsyannikov, "Parameters of cnoidal waves," in: Problems in Mathematics and Mechanics [in Russian], Nauka, Novosibirsk (1983).

NUMERICAL STUDY OF THE ACTION OF A SHOCK WAVE ON AN OBSTACLE SCREENED BY A LAYER OF POROUS POWDER MATERIAL

A. G. Kutushev and D. A. Rudakov

UDC 532.529:518.5

Currently for a number of branches of modern technology there is a very important problem of mathematical modeling for the process of shock wave operation on an obstacle shielded by a layer of loose material. In particular the requirement of solving this problem is encountered in pneumatic transport of loose materials with creation of a system for explosion protection of trunk lines, in powder technologies, in explosive processing of materials, and in safety techniques with analysis of the efficiency of protecting units screened by free-flowing layers.

The problem of studying the effect of porous shields on the reaction of shock waves with a rigid surface has been considered in [1-4] where it is shown that the maximum pressure amplitude at an obstacle shielded by layer of porous material may exceed considerably the pressure of a normal reflected shock wave from the wall of an obstacle in the absence of a porous layer. In [1, 2] in order to explain the behavior of the shielding layers of porous shields of the polyurethane type (solid porous coating with a porosity of ~97%) with passage through the layer of shock waves with Mach number ~2 a very simple model of an effective gas is used. In [3] the effect is studied of a layer of polyurethane foam on the maximum excess pressure behind the shock wave reflected from the wall using in contrast to [1, 2] models describing shield porosity: a shielding porous layer is represented by an equivalent mechanical system with one degree of freedom from a load of mass m and a combination of ideally plastic and elastic elements. Results are given in [4] for an experimental study of the parameters of shock waves reflected from a solid wall coated by a layer of porous loose material. A similar model of a porous specimen is used in order to describe the behavior of the pressure amplitude at an obstacle.

A detailed analysis is provided in this work for the process of shielding an obstacle by a layer of loose material within the scope of a two-phase model of powder material.

1. Basic Equations. In order to describe movement of a gas and porous powder material represented by a mixture of solid particles in contact with each other and gas in pores

Tyumen. Translated from Prikladnaya Mekhanika i Tekhnicheskaya Fizika, No. 5, pp. 25-31, September-October, 1993. Original article submitted March 11, 1992; revision submitted September 12, 1992.

 0021-8944/93/3405-0618$12.50